RUHR-UNIVERSITÄT BOCHUM

MATERIALS RESEARCH DEPARTMENT

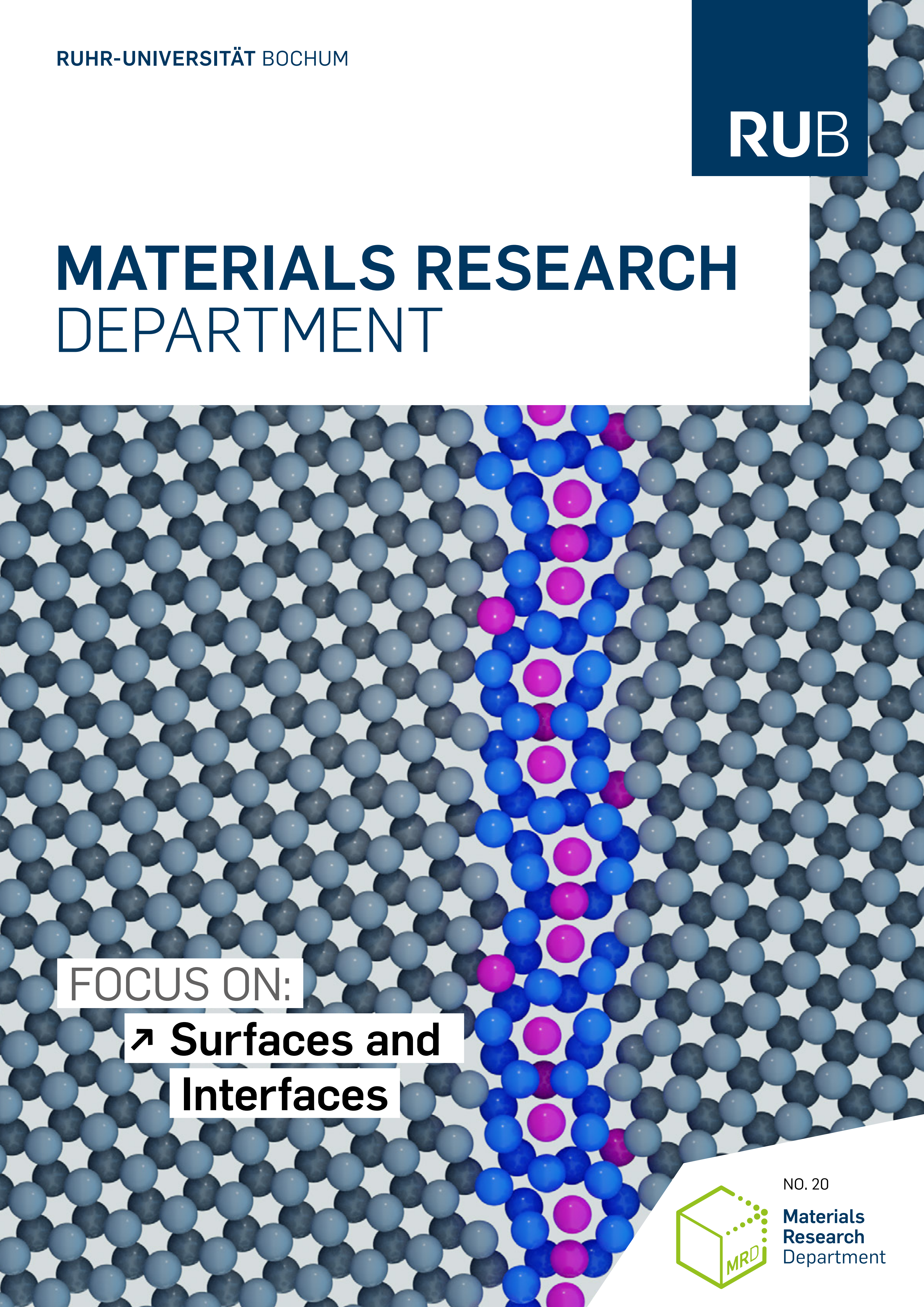

FOCUS ON:

↗ Surfaces and Interfaces

NO. 20

Materials Research Department

MRD
MATERIALS RESEARCH
DEPARTMENT

FOCUS ON:
SURFACES AND INTERFACES

The fascinating world of surfaces and interfaces lies at the heart of many key advancements in materials science. From catalysis and corrosion to adhesion and thin-film technologies, understanding how atoms and molecules behave at boundaries opens the door to innovation across a wide range of disciplines.

In this 20th anniversary edition of the MRD Newsletter, we dive into the latest discoveries, trends and research focused on these essential features.

As with all previous editions, this issue is also available on the MRD website: www.mrd.rub.de.

We look forward to your feedback and welcome suggestions for the next issues.

Enjoy reading,

Ralf Drautz and Tong Li
MRD Speakers
Anastasiia Petrova and Denisa Voicu
MRD Science Managers

CONTENT

On the cover: Simulation of icosahedral grain boundary phase formation, authors: Timofey Frolov, Christian Liebscher

HYDROGEN **AT GRAIN BOUNDARIES IN** FERRITIC STEEL **MICRO-STRUCTURES**

DFT insights on trapping and decohesion

Hydrogen embrittlement (HE) is a fundamental problem in materials science. The term summarizes several effects of H with a negative impact on the mechanical properties of structural materials such as iron and iron alloys. This impact is often due to H interaction with those defects in the material which are relevant for mechanical deformation. Therefore it is important to understand and to be able to predict the solution, respectively trapping of H at vacancies, dislocations, grain boundaries, and in areas of residual strain in the microstructure or the stress field of crack tips.

In our work, we put a strong focus on grain boundaries, since they play a dual role in HE: They are known to be likely trapping sites for H and can thus remove diffusible H from the microstructure and prevent it from causing harm elsewhere. On the other hand, they are often the weak links in the microstructure, and this tendency is enhanced by H segregation to the grain boundaries – in other words, grain boundaries are prone to hydrogen enhanced decohesion (HEDE). Both, the segregation behaviour of H at grain boundaries and its effect on the cohesive strength of the interface can be influenced by adding alloying elements to the structure. Our research aims at understanding and predicting these alloying and co-segregation effects at grain boundaries in ferritic steel. We

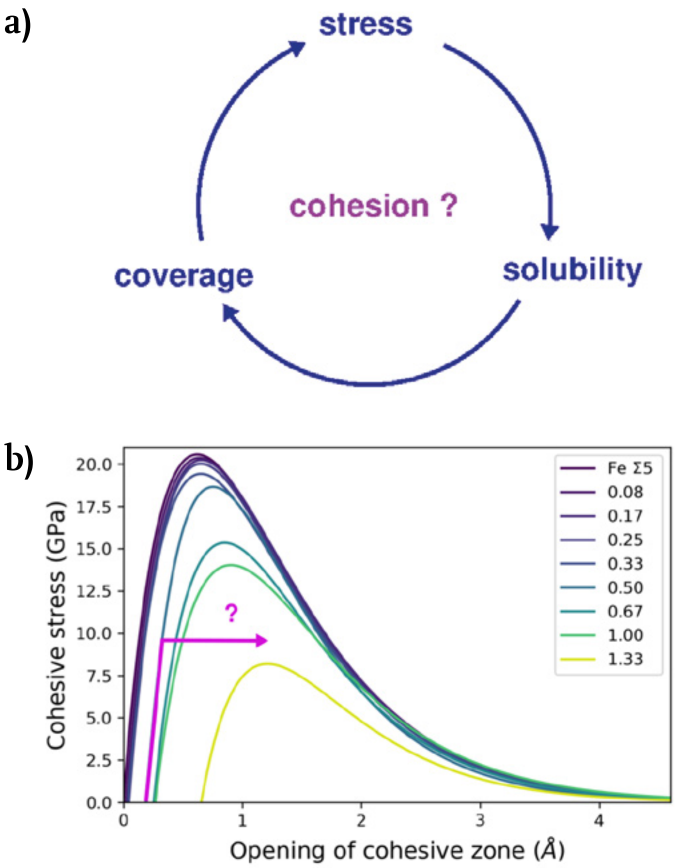

Figure 1: a) Schematic of the interdependency of stress in the microstructure, H solubility (e.g. at a grain boundary) and equilibrium coverage of the grain boundary with H. b) Cohesive stress as a function of the opening of a cohesive zone at a Σ5 grain boundary in bcc iron for different coverages of the interface with H.

would like to resolve the relation between stress, solubility and local hydrogen concentration to be able to predict the H distribution among different grain boundaries (and in the long run also other types of defects) in the microstructure. Figure 1a) shows this relation schematically: The stress state of the microstructure determines the H solubility and thus the equilibrium coverage of the defect, in this case the grain boundary. The presence of H at the grain boundary releases some of the stress and thus alters the solubility again. At the same time, H changes the cohesive strength of the interface, as shown in Figure 1b), thus it could happen that by H segregation, the grain boundary fails although the applied/local stress is below its cohesive strength in the pure state.

To shed light on this interdependency, *ab initio* density functional theory (DFT) calculations are a powerful tool, since they provide quantitative information like solution and trapping energies based on the electronic structure. By calculating the solution energy of H as a function of the hydrogen chemical potential, we can also connect them with experimentally accessible parameters (such as the H partial pressure).

As an example, we show here the results for two symmetrical tilt grain boundaries (STGBs) in body-centered cubic iron. These were chosen as models for different types of GB environments: The Σ5(310)[001] STGB represents a medium-energy, open GB structure, and the Σ3(112)[1-10] STGB a low-energy, close-packed one. To predict how the local concentration of hydrogen changes under mechanical load we initially calculated the solution energy for a single H atom in different strained states of these GBs. Figure 2 shows the solution energy surface in a plane perpendicular to the Σ5 grain boundary with excess lengths corresponding to 0, 3, and 10% elongation. With increasing strain at the grain boundary, not only the number but also the distribution of favorable sites for hydrogen was found to change. At higher elongation, new low-energy sites appear, suggesting that the grain boundary can accommodate more hydrogen atoms than previously assumed. However, to predict the actual concentration of hydrogen at the GB, one must take into account the interaction of hydrogen atoms and calculate the solution energy as a function of coverage.

Thus, using the identified sites, we investigated how increasing hydrogen coverage affects the solution energies and in turn the cohesive properties of grain boundaries. Figure 1b) shows that for the Σ5 grain boundary, the cohesive strength decreases significantly with increasing coverage, reaching up to 60 percent reduction relative to

Dr. Abril Azócar Guzmán
Materials Data Science and Informatics, Forschungszentrum Jülich
a.azocar.guzman@fz-juelich.de

PD Dr. habil. Rebecca Janisch
Mechanical Properties of Interfaces, ICAMS
rebecca.janisch@rub.de

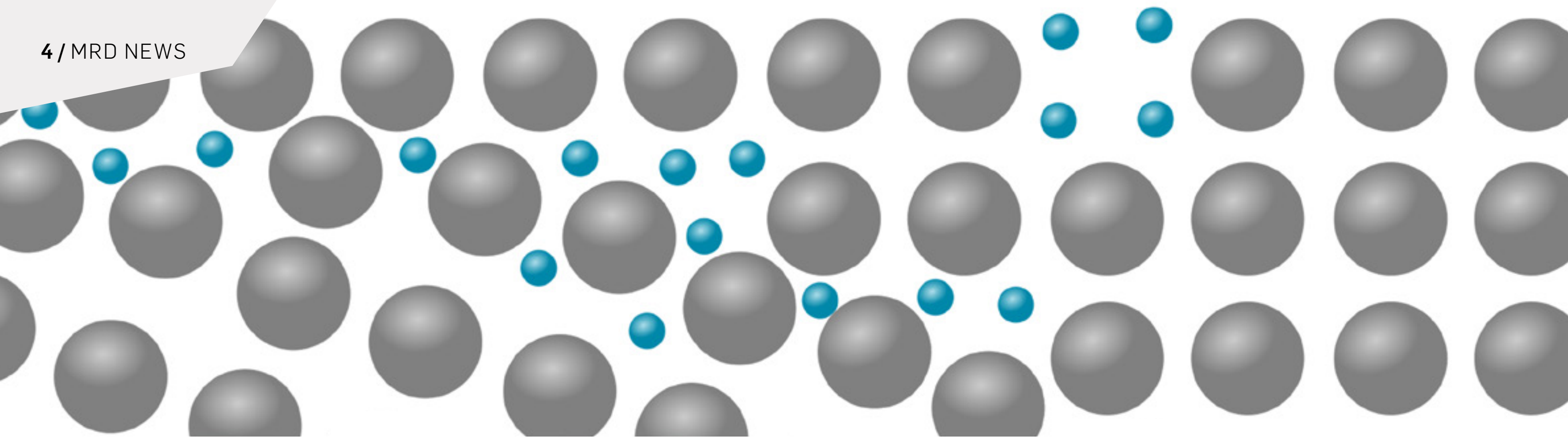

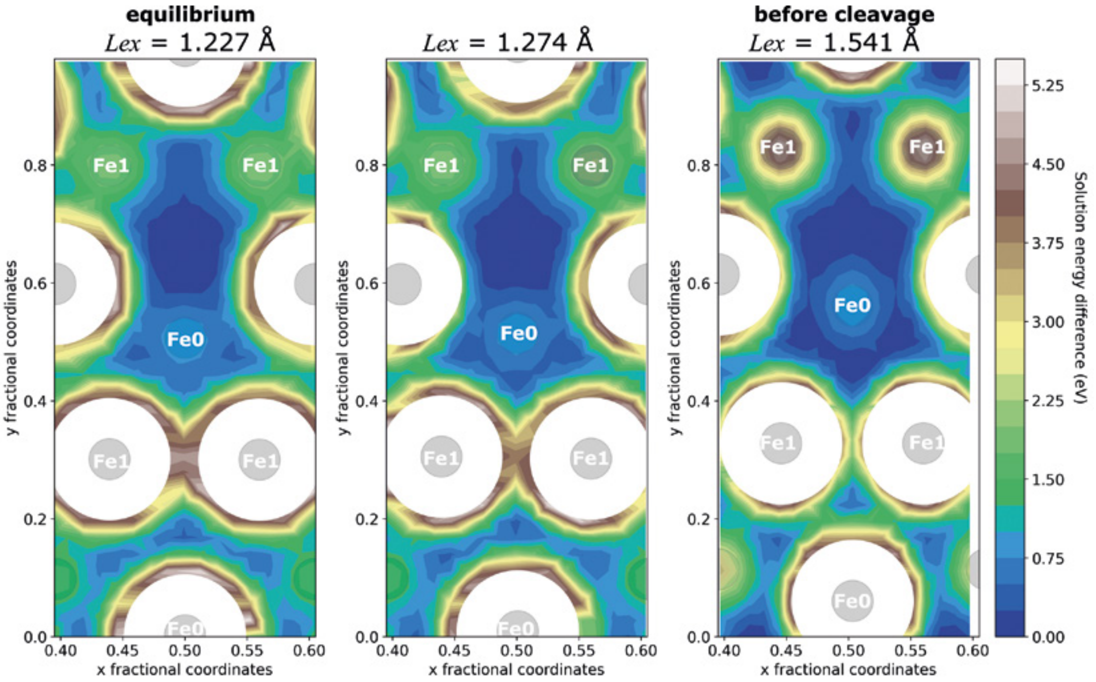

Figure 2: Cross-section of the solution energy surface for H at the Σ5 STGB in Fe in a range of ±2 Å from the GB plane in the x direction, for different strain states. The solution energy is given w.r.t. the respective lowest energy position in each case. Large white circles indicate the presence of Fe in the same plane, smaller circles labelled with Fe1 or Fe0 mark the projection of the Fe positions in neighboring planes.

the hydrogen-free case. In contrast, the Σ3 grain boundary (not shown) remains more resistant, with only a 16 percent reduction under comparable conditions. This fact alone – that the more open structure is more sensitive to H enhanced decohesion – is not too surprising, but the more interesting insight was made when we also investigated the solution energy as a function of the stress and chemical potential, closing the loop in Figure 1a). A key finding is that hydrogen solubility at the Σ3 grain boundary is significantly less affected by changes in chemical potential and applied stress than at the Σ5 grain boundary, where solubility of H for higher concentrations than 0.08 coverage drops sharply as the cohesive strength is approached. As the chemical potential is increased, hydrogen tends to accumulate at the Σ3 grain boundary under strain, always assuming that the diffusion of H happens faster than the separation process. This behavior is further influenced by the decreasing energy barriers at the Σ5 grain boundary under increasing separation, making hydrogen traps shallower.

Another crucial ingredient are the alloying elements in ferritic steels and their impact on segregation and cohesion. The addition of carbon, which is likely to segregate leads to a significant increase in cohesive strength, particularly for the Σ5 grain boundary, where strength improved by up to 45 percent. However, when hydrogen and carbon decorate the GB plane simultaneously, the overall effect becomes more complex and at higher coverages the embrittling impact of hydrogen outweighs the cohesive benefits of carbon. In all tested cases, grain boundaries with both hydrogen and carbon remained weaker than those with carbon alone.

As an example, Figure 3 shows the cohesive

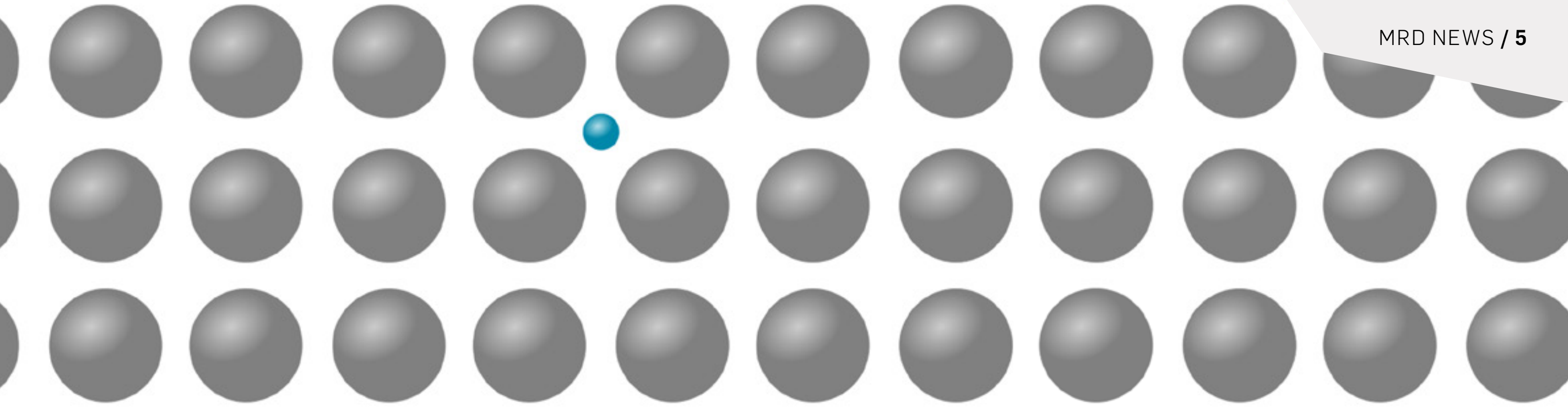

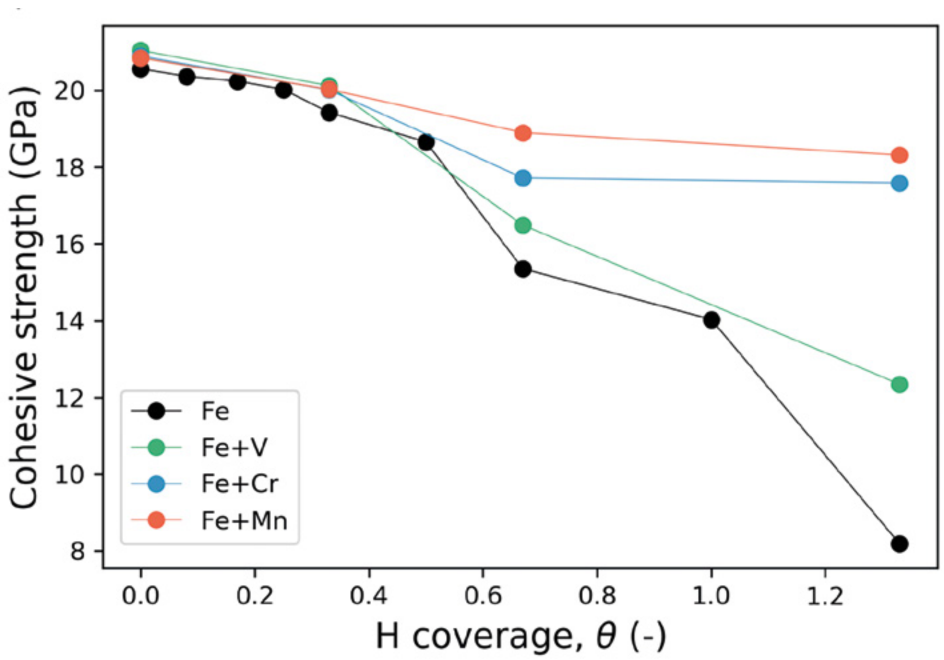

Figure 3: Cohesive strength w.r.t. hydrogen coverage of the Σ5 grain boundary decorated with alloying elements: V, Cr, and Mn.

strength of the Σ5 STGB segregated with alloying elements vanadium, chromium, and manganese as a function of hydrogen coverage. At low hydrogen concentrations, their effect is minor. At higher concentrations, however, they can significantly improve the cohesive strength of the Σ5 grain boundary. Manganese is identified to be most effective at mitigating the detrimental effect of hydrogen. This finding is consistent with experimental observations in manganese-rich steels, which tend to show improved resistance to hydrogen embrittlement, particularly at grain boundaries enriched with manganese.

In conclusion, the embrittling effect of hydrogen segregation in ferritic steel grain boundaries is strongly influenced by the local atomic arrangement, hydrogen concentration, and applied stress. Grain boundary susceptibility to hydrogen-enhanced decohesion can not be evaluated by considering isolated hydrogen atoms or idealized grain boundary models. Instead, a more realistic understanding must include local hydrogen coverage, effect of stress, and the influence of alloying elements. The analysis of the selected symmetrical tilt grain boundaries shows that more open boundary structures are more susceptible to hydrogen-enhanced decohesion. However, under tensile stress, hydrogen segregation can shift toward more stable grain boundaries, reducing the overall weakening effect. Furthermore, alloying elements such as carbon and manganese offer viable strategies to improve grain boundary strength and reduce the effects of hydrogen. By combining first-principles modeling with physically meaningful parameters, we can improve our understanding of hydrogen-enhanced decohesion and offer atomistic insight into the behavior of ferritic steel microstructures in hydrogen-rich environments.

REFERENCES:

Apart from Figure 1a) the figures in this article are adapted and reprinted with permission as granted by the creative common license CC BY 4.0 from:
Azócar Guzmán, A., & Janisch, R. (2024). Effects of mechanical stress, chemical potential, and coverage on hydrogen solubility during hydrogen-enhanced decohesion of ferritic steel grain boundaries: A first-principles study. Physical Review Materials, 8, 073601.

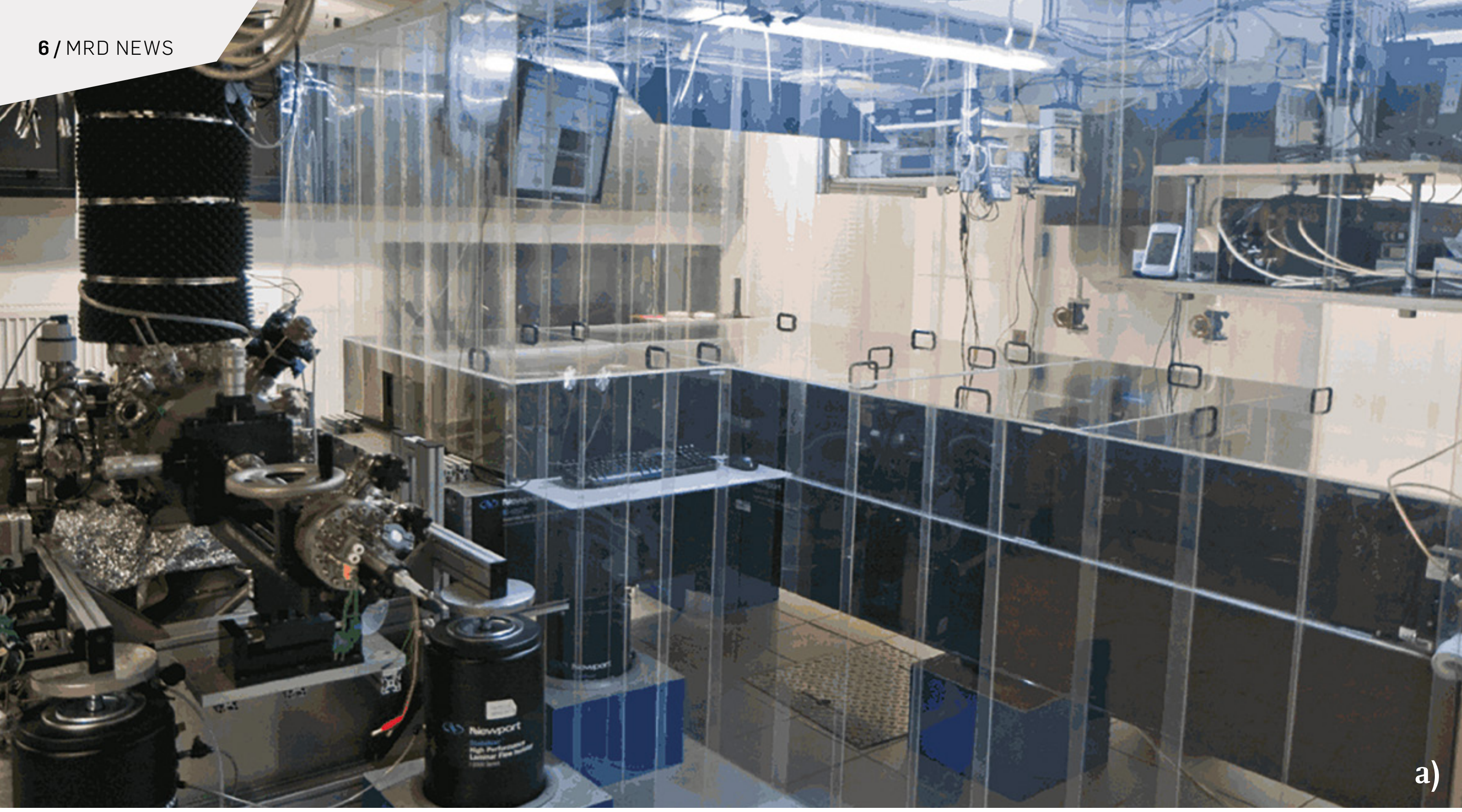

IMAGING **LASER-INDUCED SURFACE RESTRUCTURING** ON THE **NANOSCALE**

Bridging the gap between academic and industrial research

Prof. Dr. Karina Morgenstern
Physical Chemistry I
karina.morgenstern@rub.de

While material processing by powerful ultra-fast lasers is well-established and even used industrially, it is a topic of current research on how the interaction between light and the material causes microscale changes. Moreover, at laser intensities far below the ablation threshold (absorbed fluences below 5 mJ/cm^2 with 'fluence' representing the amount of energy deposited per unit area), the surface has been considered unaltered in femtochemistry [1], an assumption used to model chemistry induced by laser light on surfaces. Our results falsified this assumption for coin metals through a novel multi-scale approach, extending the nanoscale resolution of a low-temperature scanning tunneling microscope to the microscale [2, 3].

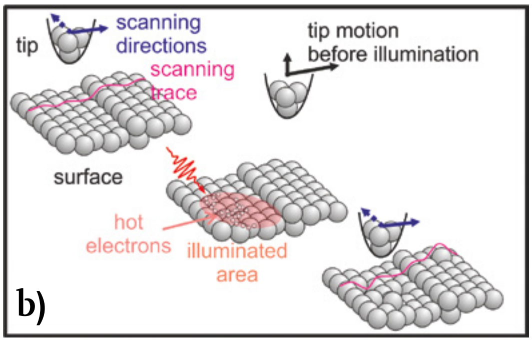

Figure 1: Picture of the experimental set-up (a) and schematics of the three steps experimental procedure (b).

The interaction of fs laser pulses with metals and how it induces chemistry on its surfaces is well-established [1]. It is the electron system of the sample that absorbs the laser light. Each photon lifts an electron from the occupied to unoccupied states, creating a non-equilibrium hot electron/hole distribution. Through inelastic scattering, the distribution equilibrates quickly to an equilibrium distribution corresponding to an electron temperature far above the phonon temperature. These hot electrons or holes can transfer into adsorbates to excite them to reactions. While averaging methods have been used extensively, there has been very little information about the nanoscale variation of the induced processes before our work [4, 5]. Initiated by these pioneering studies, we designed and implemented a combination of a low-temperature STM with a femtosecond laser [6] to investigate the influence of ultra-short laser irradiation in real space (Figure 1). The system has been used at fluences below 0.5 mJ/cm^2 in chemical research for non-adiabatic hydrogen bond reorientation within water clusters [7], CO_2 formation [8], and CO diffusion [9].

At slightly higher fluences, we investigate changes to the Ag(100) surface induced by ultra-short laser pulses by scanning tunneling microscopy [2]. We unravel that the surface is restructured on the nanoscale contrary to expectation (Figure 2) with nanoscale clusters (white protrusions) and vacancies (black depression). Imaging the same surface region repeatedly before and after laser irradiation at increasing fluence (Figure 2 a to d) yields highly non-linear yields (Figure 2 e, f). A thorough analysis of the restructuring reveals its origin, vacancy-interstitial formation in the bulk and laser-driven diffusion of vacancies and interstitials to the surface [2].

The intensity and, with it, the fluence of a laser spot varies with a Gaussian profile. Averaging methods necessarily average across a broad range of fluences. Our method revealed that the surface restructuring varies substantially in size and shape across the laser spot (Figure 3) [3]. Small compact and larger dendritic islands are formed at low (region III) and high fluence (region I) on the Cu(111) surface, respectively, and mixtures at intermediate fluence (region III). Abrupt alterations of the laser-created structures indicate yet-unrevealed non-adiabatic processes [3]. This local dependence on the micrometer scale has been mostly ignored so far, both in research and application. We revealed three neglected effects in light-matter interaction: changes below ablation, local variations across a laser spot, and non-continuous variations. Our study highlights the importance of local imaging for understanding the effect of ultra-short heating of the electron system on material during ultrafast laser irradiation and relating specific structural changes to the local fluence. The influence of the three effects of ultra-fast laser light on nanoscale structures is a topic of interest in materials engineering, impacting practical applications beyond the engineering of nanostructures, in particular processes where these materials are used, e.g., in heterogeneous catalysis. Moreover, the developed method to characterize the nanoscale structures across a micro-sized laser spot opens the possibility of discovering other not-yet-considered variations in structural changes.

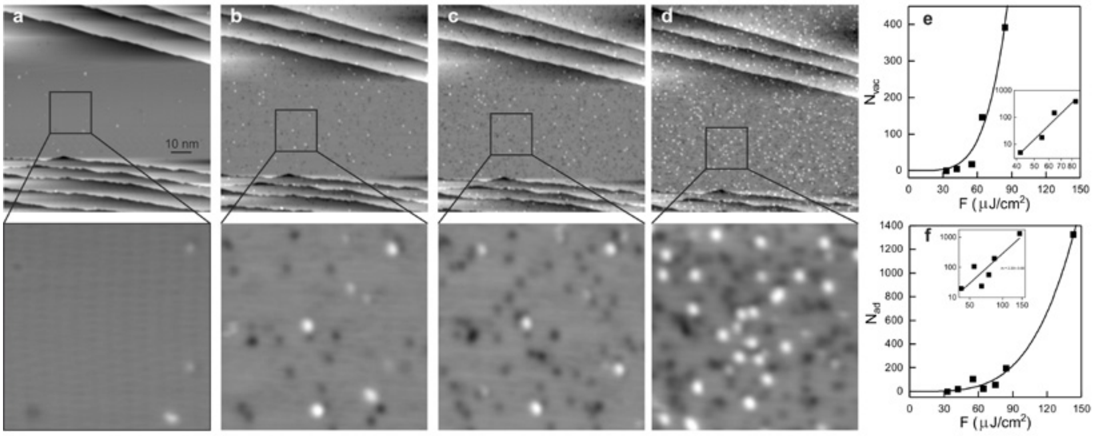

Figure 2: Fluence dependence: (a to d) Series of fs-laser irradiation (50 fs, 400 nm) of the same Ag(100) surface region with increasing fluence (upper row) with zooms (lower row) (e, f) number of laser-created clusters (e) and holes (f) per 1000 nm^2 vs. absorbed fluence; from [2].

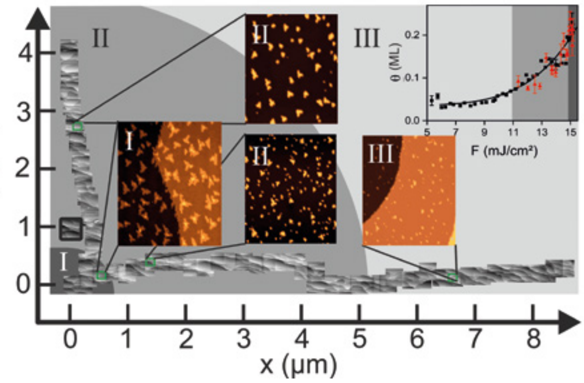

igure 3: Micrometer-scale imaging across the aser spot: 90 adjacent STM images (greyish quares) covering a range of 8.5 μm in the x irection and 4.1 μm in the y direction with on xemplary image enlarged for regions I, II, and II (different shades of gray); inset: coverage Θ s. local fluence F in x (black squares) and y irections (red triangles) with fit; from [3].

REFERENCES:

1 Frischkorn C., and Wolf M., Chemical Reviews (2006), 106, 4207.

2 Zaum C., et al., Scientific Reports (2021), 11, 13269.

3 Osterloh N., et al., Nanoscale Horizon (2023), 8, 55.

4 Dürr M., et al., Science (2002), 296, 1838.

5 Bartels L., et al., Science (2004), 305, 648.

6 Mehlhorn M., et al., Review of Scientific Instruments (2007), 78, 033905.

7 Mehlhorn M., et al., Physical Review Letters (2009), 103, 026101.

8 Gawronski H., et al., Angewandte Chemie International Edition (2010), 49, 5913; Angewandte Chemie (2010), 122, 6049.

9 Zaum C., et al., Physical Review Letters (2015), 114, 146104.

THERMAL SPRAY AS A POWERFUL **COATING TECHNOLOGY** FOR DIFFERENT **ENERGY SYSTEMS**

Examples of coatings for energy application

Thermal spray is a coating technology which is used in numerous applications for the deposition of rather thick ceramic or metallic coatings. In this process, powderous feedstocks in the size range of several 10 micrometers are accelerated and heated in a hot and fast gas jet. When the particles impinge on the substrate, they produce a lamellar structure. Ceramic coatings are often full of microcracks and pores due to the fast cooling after deposition and the brittle nature of the feedstock. These microstructural features are often beneficial for high temperature applications e. g. as thermal barrier coatings (TBCs) in gas turbines as they reduce effectively stress levels during thermal cycling. Figure 1a shows the fracture surface of an atmospherically plasma sprayed (APS) yttria stabilized zirconia (YSZ) thermal barrier coating (TBCs) with cracks within and between the sprayed lamella. This strain tolerant microstructure can be even further improved by implementing columnar structures in the coatings (Figure 1b). The gaps between the columns can open during heating of a component leading to a strain-tolerant coating. Such coatings can be produced by suspension plasma spraying (SPS) in which suspensions are introduced in the plasma jet instead of particles. As the droplet size is then much lower, the droplets can now follow the gas flow of the jet only impinging on surface obstacles where the columns grow. We could demonstrate that the full use of such coating systems can only be made, if a peroxidation of the underlying bond coat is made before coating deposition [1]. Such coatings have then a more than twofold better thermal cyclic performance as conventional APS coatings.

Also SiC/SiC composites as advanced structural materials for high temperature applications need protective coatings when being used in gas turbines. Here the water vapor corrosion plays an important role as it leads to evaporation of the typically on SiC formed silica scale and hence the corrosion of the hole component. This degradation can be significantly reduced by different coatings e. g. made of $Yb_2Si_2O_7$. This so-called environmental barrier coatings (EBCs) are also mainly applied by atmospheric plasma spraying. Major issues are here the micro-cracked and hence not gas-tight as well as amorphous microstructure of the APS coatings. Crystallisation at high temperatures leads to shrinkage and crack formation. Here we could demonstrate that with very low pressure plasma spraying (VLPPS) dense and crystalline coatings can be produced [2].

A self-healing chrome evaporation barrier which is used to prevent Chrome poisoning in solid

Prof. Dr. Robert Vaßen
Materials Synthesis and Processing, Forschungszentrum Jülich
r.vassen@fz-juelich.de

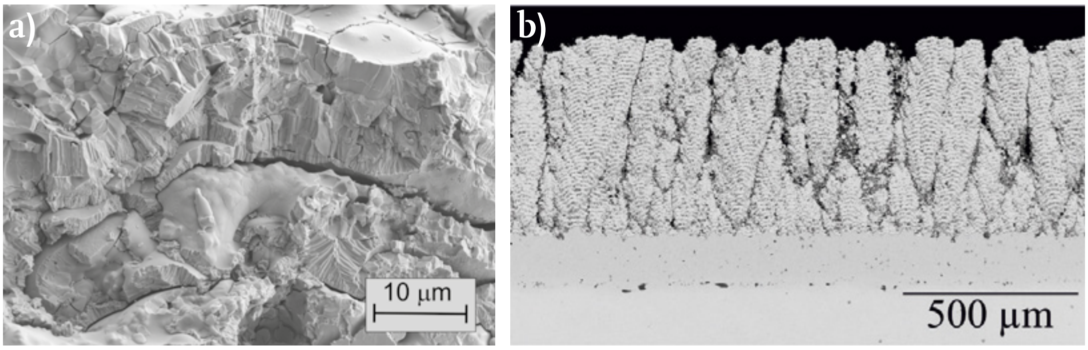

Figure 1: Fracture surface of an APS coating (a), cross-section of columnar coating prepared by SPS (b).

oxide fuel cells (SOFCs) can be made of a MnCoFe oxide spinel. It is often deposited by APS which leads to a microcracked, porous coating. The Cobalt is reduced during spraying and so a simple rock salt structure is formed. During operation in air above 500°C the structure takes up again the oxygen. The accompanied volume expansion closes the cracks in the coatings and leads to an extremely protective coating (Figure 2)[3].

In addition to the shown ceramic coatings also metallic coatings can be produced by thermal spray. As first example in Figure 3 a graded tungsten/ferritic steel coating is shown. This type of coating is a candidate for the first wall of a fusion reactor. The gradient helps to compensate the large mismatch between the thermal expansion coefficients of the structural material made of ferritic steel and the plasma facing tungsten [4]. A favourable way to produce this structure is by vacuum plasma spraying. Although the in-plane stress in the top layer is hardly affected, the thickness of the deformed layer at the interface is enlarged and so the damage is no longer localized. This concept can also be transferred to real components and was 2022 awarded with the SOFT Innovation Prize by the European Commission [5].

Another important field of application for thermally sprayed coatings is the water electrolysis. We could demonstrate within the HyInnoCells project in the Zukunftscluster Wasserstoff at RWTH Aachen that in PEM electrolysis cold sprayed titanium coatings on stainless steel expanded metal could substitute porous transport layer (PTL) completely made out of titanium and hence reducing the titanium consumption [6]. In the now started HyInnoLyze2 project this is further developed and in addition newly identified, extremely corrosion resistant alloys – a patent was just filed – will be further improved. Here also combinatorial approaches using PVD technology to manufacture large amounts of different compounds will be used to screen and optimize corrosion properties. Finally, it could be demonstrated that thermal spray can be used for the manufacture of complete cells for alkaline electrolysis, this will be in depth investigated in the BMWK project Kadise.

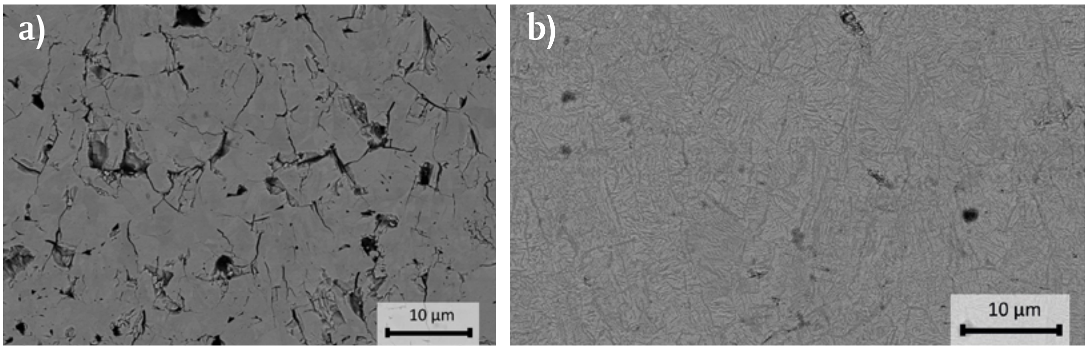

Figure 2: Self-healing MnCoFe-oxide coating in the as-sprayed condition (a) and after heat treatment (500°C, 4h, b).

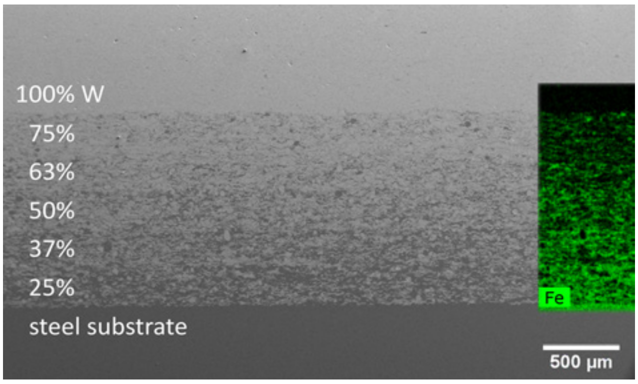

Figure 3: Graded tungsten-ferritic steel coating developed for the first wall of fusion rectors applied by vacuum plasma spraying.

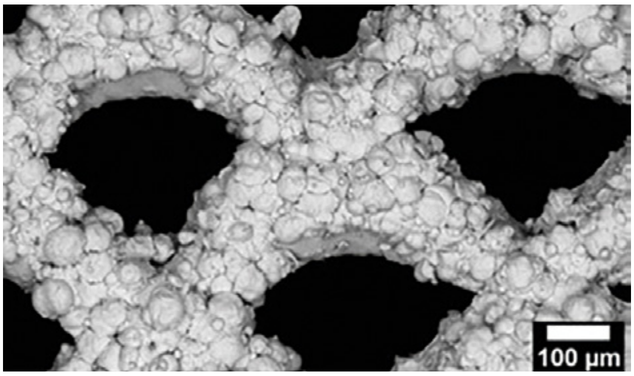

Figure 4: A cold gas sprayed Titanium coating on an expanded stainless steel metal as porous transport layer for PEM electrolysis.

REFERENCES:

1 Joeris J., et al., Coatings (2023), 13 (9).
2 Vassen R., et al., Coatings (2019), 9 (12).
3 Grünwald N., et al., Journal of the European Ceramic Society (2019), 39 (2), 449-460.
4 Grammes T., et al., Fusion Engineering and Design (2023), 188, 113430.
5 https://research-and-innovation.ec.europa.eu/news/all-research-and-innovation-news/soft-innovation-prize-three-researchers-awarded-2022-09-19_en.
6 Sievert T., et al., Surface and Coatings Technology, submitted.

HYDROGEN PERMEATION **BARRIER COATINGS FOR A** HYDROGEN-BASED GREEN **ECONOMY**

Preventing hydrogen embrittlement using protective alumina coatings

Hydrogen has emerged as a key fuel in advancing the green economy and addressing climate change, driven by rising CO_2 emissions from carbon-intensive processes. Suitable hydrogen storage and transport infrastructure, such as steel tanks or pipelines, is essential to integrate hydrogen into the economy. However, these systems require protection against *hydrogen embrittlement (HE)*, a phenomenon where hydrogen atoms infiltrate the metal's crystal lattice and degrade its mechanical properties by interacting with microstructural features such as vacancies, dislocations, cracks, grain/phase boundaries, or forming brittle hydrides. At the Max Planck Institute for Sustainable Materials, research is focused on uncovering the atomic-scale mechanisms of hydrogen interactions [1] and developing surface protection strategies to mitigate HE.

A central aspect of our strategy to prevent HE involves modifying metallic surfaces by adding protective *hydrogen permeation barrier (HPB) coatings* [2–4]. These coatings are designed to minimize the hydrogen uptake by exhibiting low permeability, solubility, and diffusivity for hydrogen. To be effective, HPB coatings must also exhibit strong adhesion and mechanical compatibility with the substrate, and minimal defects such as microcracks or pores. Promising candidate materials include ceramic oxides, nitrides, carbides, and multilayer ceramic composites, all known for their low hydrogen permeability [3, 4]. The performance of HPB coatings is critically linked to their chemical composition, deposition technique, and resulting microstructure, which can be amorphous, polycrystalline or columnar-grained [3].

In collaboration with academic and industrial partners, we are developing innovative strategies for coating and characterizing HPB layers on commercial aluminum alloys and steels. Specifically, we are investigating Al_2O_3 coatings prepared by different methods, resulting in either amorphous or nanocrystalline coatings. Al_2O_3 is highly attractive as HPB material due to its extremely low hydrogen permeability ($\sim 10^{-17}$ $mol/(m.s.Pa^{0.5})$), and superior permeation reduction factor compared to many other ceramic coatings. To mitigate HE in steels,

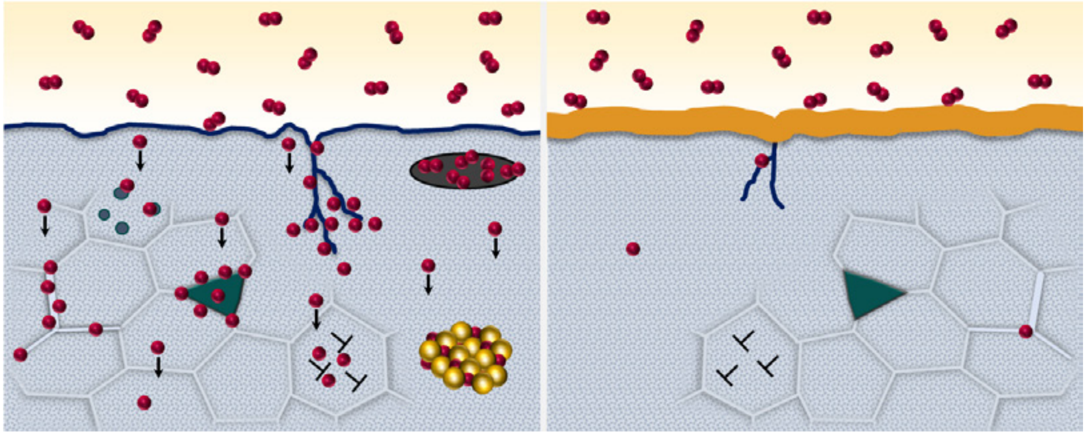

Figure 1: Schematic illustration showing the interaction of hydrogen (red circles) with different features in the crystal lattice after its absorption in an uncoated material (left), while such hydrogen ingress is remarkably minimized by the addition of a barrier coating on the surface (right).

amorphous Al_2O_3 coatings up to 2 µm thick were deposited on the surface of an Fe-Cr alloy using plasma-ion assisted deposition [2]. The addition of this amorphous Al_2O_3 layer greatly improved the alloy's resistance to hydrogen penetration, with the coating's diffusion coefficient being nine orders of magnitude lower than that of the uncoated material. This substantial reduction further strengths a material's resistance to hydrogen embrittlement, increasing their durability in hydrogen-exposed environments. In a follow-up project Al_2O_3 coatings are applied on a commercial Al 6082 alloy using an electro-chemical oxidation (ECO) technology developed by our industry partner. This technique produces thick (~15 to 30 µm) nanoceramic, conformal coatings through anodic oxidation in the presence of plasma micro-arc discharges. The localized high temperatures generated during the process promote the formation of crystalline Al_2O_3, which is required for achieving excellent wear resistance as well as mechanical and thermal stability.

Such electrochemically oxidized Al_2O_3 coatings exhibit a compact through-thickness microstructure with strong adhesion to the substrate, both essential characteristics for HPB coatings. Our studies show that the coating's composition is uniform while the microstructure evolves with thickness, transitioning from a mix of α+γ Al_2O_3 phases in thicker coatings to predominantly γ-Al_2O_3 in thinner ones (~15 µm). These changes in microstructure can impact both the mechanical properties and the hydrogen blocking performance. The microstructure features nanocrystalline grains ranging from ~200 nm to 1 µm in size, along with pores and crack networks, which are common in ceramic coatings due to residual stresses arising from thermal expansion mismatch between coating and substrate. To further improve the barrier performance, we also explore crack-sealing strategies using polymer-based sealants.

When adding a HPB coating, it is essential that the mechanical integrity of the coated system remains intact. Our tensile tests on Al 6082 alloy, both uncoated and coated with Al_2O_3, showed promising results, with tensile strength values remaining consistent in the range of ~330 to 340 MPa. Additionally, mechanical testing under hydrogen exposure, including custom-designed small-scale nanomechanical characterization of the coatings is used to determine coating properties and coating-substrate interface adhesion. For example, nanoscratch testing was employed to understand the interface failure mechanisms of the amorphous Al_2O_3 coating on Fe-Cr alloys during hydrogen exposure [2]. Our findings indicate that hydrogen accumulation at the coating-substrate interface leads to significant changes in scratch morphology and adhesion, highlighting the importance of considering hydrogen effects in the design of protective coatings for hydrogen-sensitive materials. These studies deepen our insights into how well the coatings perform under realistic conditions where HE is a concern. This research brings us one step closer to scalable, reliable solutions for hydrogen infrastructure, paving the way for a more sustainable, hydrogen-powered future.

Acknowledgement: This is part of the project Hydrogen Embrittlement Protection Coatings - HEPCO, which is financially supported by "Zentrales Innovationsprogramm Mittelstand" (project KK5571101SH3). This work is jointly supported by Mohammed Kamran Bhat, Christina Scheu, Gerhard Dehm from MPI-SUSMAT, and in collaboration with Cambridge Nanolitic Ltd., NTTF Coatings Germany and Cranfield University.

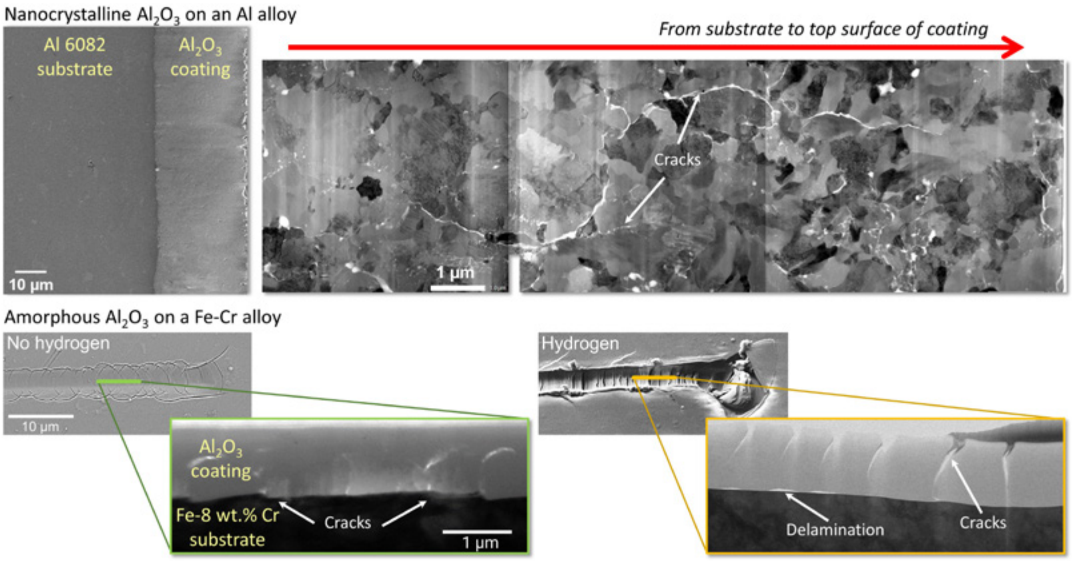

Figure 2: (Top) A scanning electron image of an electrochemically oxidized Al_2O_3 coating on Al6082 substrate (left), and a combo image of the nanocrystalline grain microstructure along the thickness, observed by transmission electron microscopy (right). (Bottom) Nano-scratch testing of an amorphous Al_2O_3 coating on a Fe-Cr alloy in air (left) and during hydrogen loading (right) to determine the coating-substrate interface adhesion.

Dr. Anwesha Kanjilal
Structure and Nano-/
Micromechanics of
Materials, MPI SusMat
a.kanjilal@mpie.de

Dr. María Jazmin Duarte Correa
Structure and Nano-/
Micromechanics of
Materials, MPI SusMat
j.duarte@mpie.de

Prof. Dr. Gerhard Dehm
Structure and Nano-/
Micromechanics of
Materials, MPI SusMat
dehm@mpie.de

REFERENCES:

1 Rao J., et al., Materials & Design (2023), 232, 112143.

2 Gopalan H., et al., Journal of Materials Research (2024), 39, 1812–1821.

3 Kanjilal A., et al., Annual Review of Materials Research (2025), 55.

4 Wetegrove M., et al., Hydrogen (2023), 4, 307–322.

QUASICRYSTALLINE-LIKE
GRAIN BOUNDARY PHASES

Building blocks for future quantum technology

Most technologically relevant materials are polycrystalline in nature, and their internal interfaces significantly affect their properties and functionality. The interfaces separating differently oriented crystals, known as grain boundaries (GBs), strongly impact the durability and overall performance of materials. Tailoring the properties of polycrystalline materials by designing the structure and composition of GBs has recently emerged as a promising pathway. Beyond being considered simple two-dimensional (2D) interfaces, it has been realized that GBs themselves can adopt distinct 2D states [1-3]. Transitions between different GB phases can be triggered by various factors, including the segregation of solutes in multi-component systems. This segregation can profoundly influence materials, ranging from causing embrittlement to providing beneficial strengthening. However, an understanding of how solutes affect the interface structure and hence GB phase transitions is lacking.

Here, we used atomic-resolution imaging and atomistic simulations to observe how iron (Fe) segregation alters the structure of GBs in hexagonal close-packed (hcp) titanium (Ti) [4]. Atomic resolution high-angle annular dark field (HAADF)–scanning transmission electron microscopy (STEM) of a pristine Σ13 [0001] symmetric tilt GB in Ti revealed a distinct periodicity with subunits “A,” “B,” and “C” [4]. These units are similar to those modeled in Ti and other ceramic-based materials. Observing a GB segment decorated with Fe at atomic resolution demonstrated a complete rearrangement of the atoms from the “ABC” configuration to isolated cage-like units in an asymmetric GB as shown in Figure 1a. The elemental

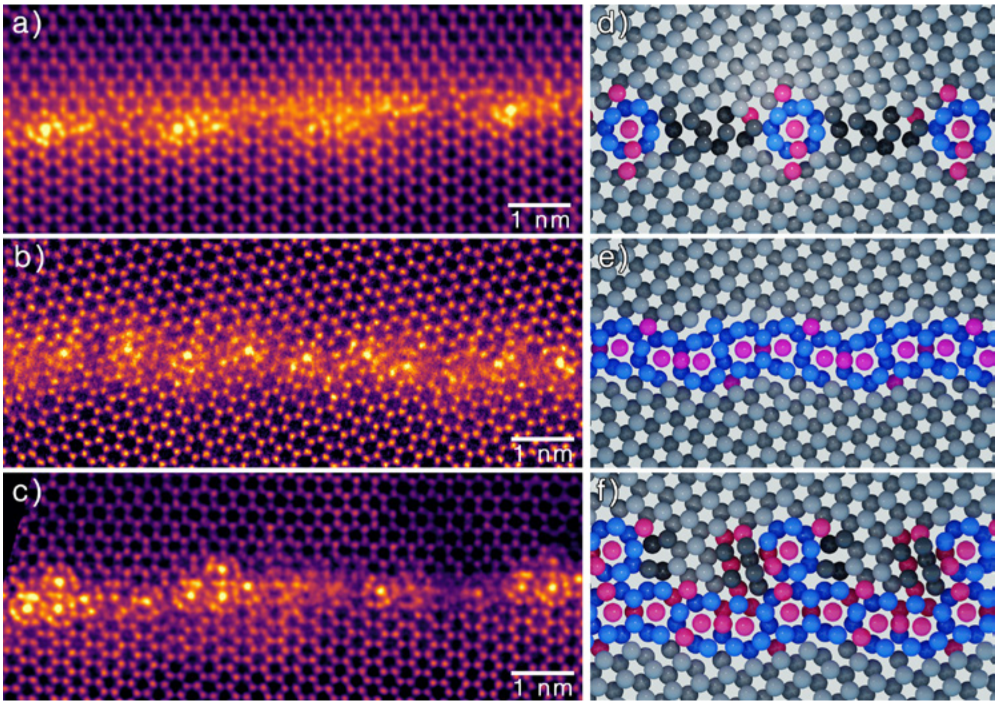

Figure 1: Experimental atomic resolution HAADF-STEM images of different cage arrangements at symmetric and asymmetric Ti GBs viewed along the [0001] tilt axis are shown in a), b) and c). The bright atomic columns represent the central Fe-rich column of the icosahedral cage structures. In a) isolated cages have formed at an asymmetric GB segment, while in b) the entire symmetric GB is decorated with cage structures and in c) cage clustering is observed. Predicted GB structures as a function of Fe concentration are illustrated in d), e) and f). The purple atoms are Fe atoms, the blue atoms highlight Ti atoms in the vertices of the icosahedral cages and the gray atoms are other Ti atoms. The Fe excess at the GB in d) is 6 atoms/nm^2, in e) 12 atoms/nm^2 and f) 26 atoms/n^2.

Prof. Dr. Christian Liebscher
Advanced Transmission Electron Microscopy, Faculty of Physics and Astronomy & Research Center Future Energy Materials and Systems
christian.liebscher@rub.de

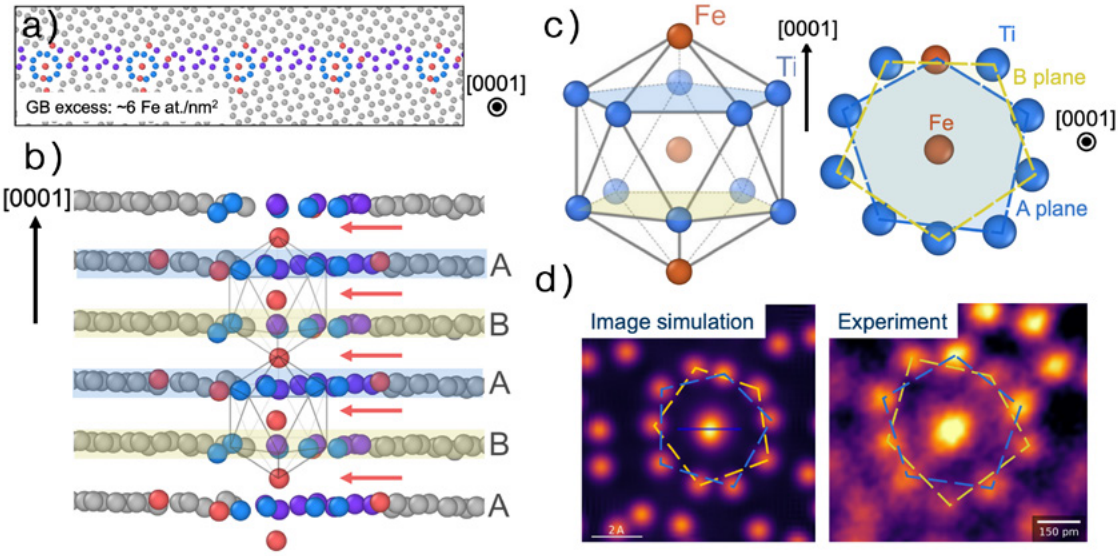

Figure 2: a) View of a predicted GB with isolated cages along the [0001] tilt axis. b) Observing this GB perpendicular to the tilt axis reveals stacking of icosahedrons as well as Fe atoms occupying interstitial positions between the A and B planes of the hexagonal crystal structure leading to a doubling in the Fe atoms (red) compared to the surrounding Ti atoms (blue). The purple atoms are other Ti GB atoms. c) View of an isolated cage showing the central Fe column and Ti atoms at the vertices of the icosahedron (left). The corresponding projection along the tilt axis (right) shows the rotated pentagons of the icosahedral structure connecting to the A and B planes, respectively. d) Comparison of a simulated and an experimental HAADF-STEM image. The central column of the cage is brighter than expected since the number of Fe atoms in this column is doubled.

contrast provided by HAADF-STEM imaging suggested that the cage center is rich in Fe, whereas the surrounding shell is rich in Ti. This observation was verified using near-atomic resolution energy-dispersive X-ray and electron energy loss spectroscopy in the STEM [4]. However, the intensity of the central Fe-rich columns is higher than expected for a fully occupied Ti column, indicating that a restructuring of the GB core also occurred along the viewing direction. At other interfaces, we even observed that cages form a layer-of-cages (Figure 1b) and that cages assemble to form aperiodic clusters (Figure 1c).

We used advanced atomistic modeling to predict the 3D structure of the icosahedral cage units and to explore the underlying nature of the segregation-induced phase transformations. Grand canonical GB structure prediction as a function of Fe composition at 0 K revealed more than five distinct GB structures. Similar to experiment, isolated cages (Figure 1d), a layer-of-cages (Figure 1e), cage clusters (Figure 1f) and even more complex cage arrangements were found [4]. These findings are supported by hybrid molecular dynamics and Monte Carlo simulations in the canonical ensemble at 300 K, where it is observed that different GB phases, represented by different cage arrangements, can transform into each other by increasing the amount of Fe in the system. With this, the total amount of Fe that can be adsorbed at the GB upon cage formation is more than twice as high compared to the pristine Ti GB structure.

The simulations provide access to the three-dimensional view of the cages as shown in Figure 2. The view perpendicular to the tilt axis of the GB shows that the cage units observed in the experiment are composed of icosahedra. They are stacked on top of each other to form a chain of icosahedrons along the tilt axis, where the Fe atoms in the central column occupy interstitial positions between the (0002) lattice planes of the hexagonal close-packed structure (Figure 2b and d). The topological properties of these icosahedral cages, described by their symmetry, dense atomic packing, and geometric flexibility, enable them to adapt to the given bicrystallography and promote the formation of several distinct GB phases characterized by different numbers of clustered icosahedral cage structures. However, their fivefold symmetry and triangulated surface net of atoms prevent them from growing into bulk phases (Figure 2c). The results show how the formation of icosahedral phases can induce new states of GBs reminiscent of glass-like or quasicrystalline structures.

Understanding the nature of phase transitions of GBs in metallic alloys induced by solute atoms is pivotal to GB structure engineering and to sculpt new materials with advanced properties. The formation of icosahedral cage structures leads to a complete restructuring of the interface. The cage units act as building blocks of distinct GB phases, explaining why more than twice the amount of Fe can be incorporated compared to the solubility limit of the initial GB. The observed topological segregation transition provides insights into solute-induced states of GBs and introduces another lever for interface design.

REFERENCES:

1 Hart E. W., Scripta Metallurgica (1968).
2 Meiners T., et al., Nature (2020), 579, 375-378.
3 Langenohl L., et al., Nature Communications (2022), 13, 3331.
4 Devulapalli V., et al., Science (2024), 386, 420-424.

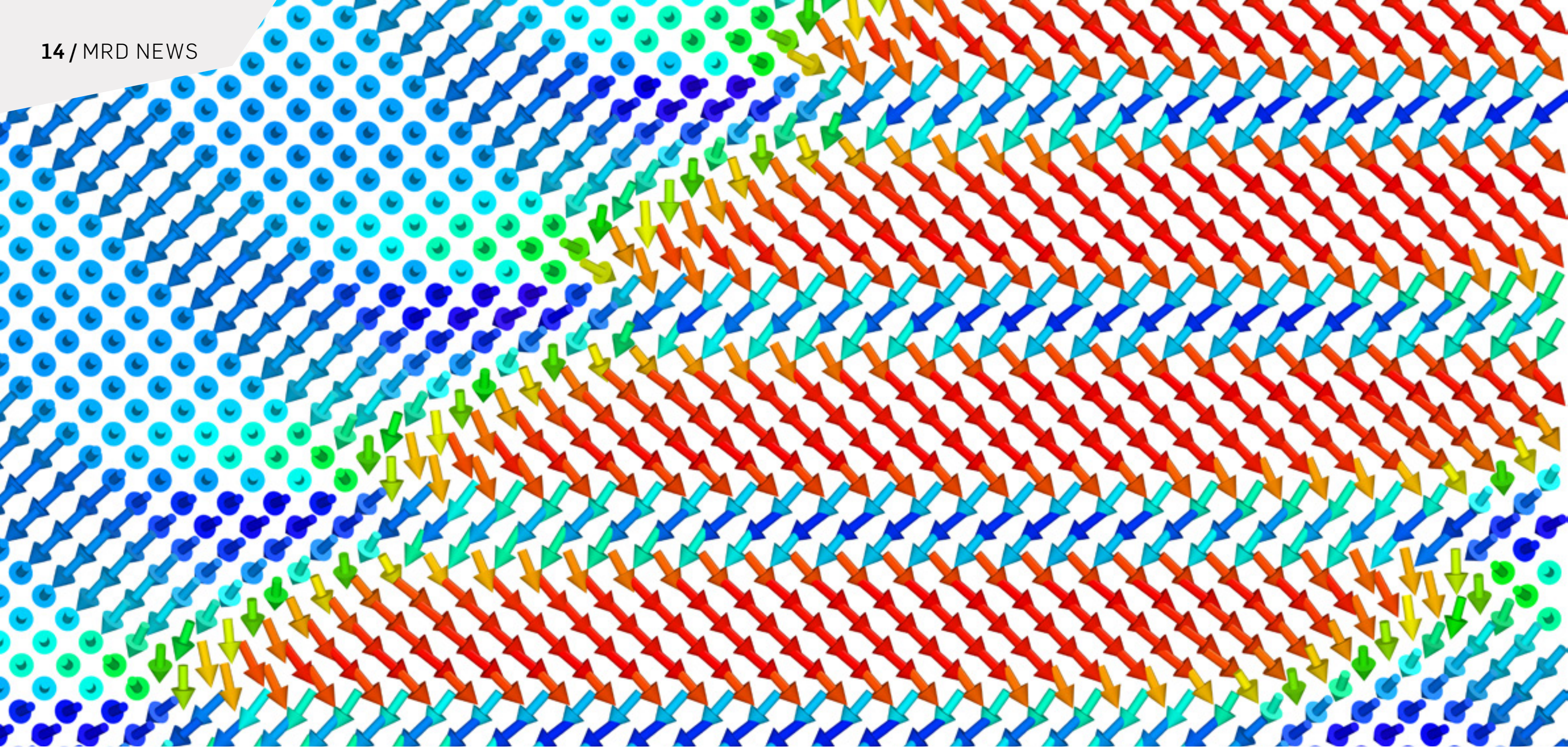

FERROELECTRIC DOMAIN **WALLS**

Towards nanoscale control of intrinsic interfaces

Prof. Dr. Anna Grünebohm
Scale-Bridging Simulation of Functional Composites, ICAMS
anna.gruenebohm@rub.de

Lan-Tien Hsu
Scale-Bridging Simulation of Functional Composites, ICAMS
lan-tien.hsu@rub.de

Ferroelectric materials, characterized by their switchable electric polarization, have long played an important role in sensors, actuators, optical and memory devices, and are promising for new computing and cooling technologies [1-4].

The underlying functional responses (pyroelectric, piezoelectric, dielectric,...) are largely governed by an important class of intrinsic interfaces: *ferroelectric domain walls*. These narrow, often atomically thin, boundaries between regions of different uniform polarization directions are far from being passive structural defects. They are tunable functional interfaces that exhibit properties that can differ dramatically from the bulk material, ranging from enhanced conductivity and magnetic ordering to chiral and topologically nontrivial states. Since ferroelectric domain walls can be written, moved, and erased by external stimuli, they offer new avenues for the nanoscale control of material properties.

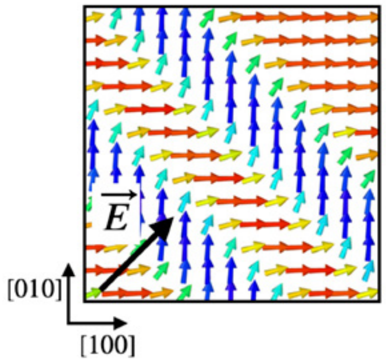

Figure 2: Example of dense domain walls induced in the tetragonal phase of $PbTiO_3$ at 635 K by a non-collinear electric field along [110] (black arrow). Each arrow represents the time-averaged local polarization and is color-encoded according to Px. Adapted from [6].

To fundamentally understand and control the microscopic properties of domain walls and their motion in ferroelectric perovskites, we utilize ab initio-based coarse-grained models and molecular dynamics simulations. Figure 1 illustrates the field-induced motion of domain walls in the orthorhombic phase of $BaTiO_3$. The field is applied parallel to the polarization direction of the red domain, which grows at the expense of the antiparallel black domain through wall motion. Microscopically, clusters of dipoles with a switched direction nucleate and grow in front of the moving wall. Interestingly, this switching occurs in a two-step

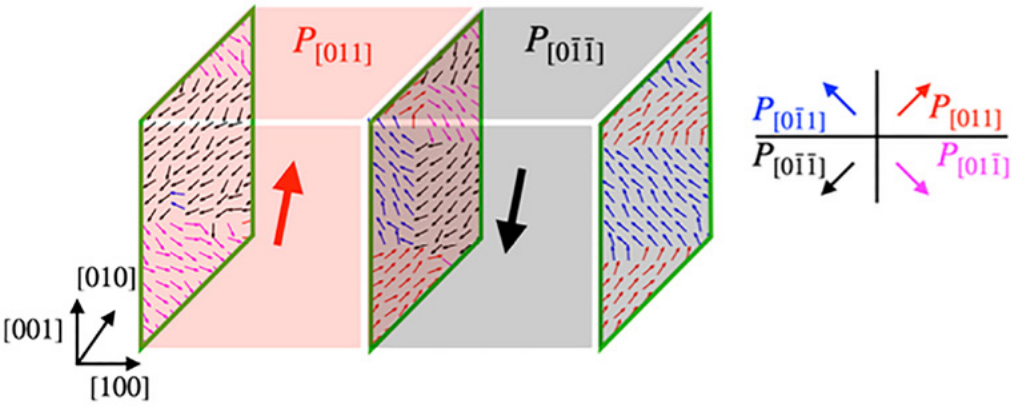

Figure 1: Schematic illustration of the complex dipole pattern on moving 180° walls in the orthorhombic phase of $BaTiO_3$. In an applied electrical field along [011], domains with parallel polarization direction (red) grow, while the antiparallel domain (black) shrinks by the motion of domain walls (green). Two successive 90° switching steps via [0-11] (blue) and [01-1] (magenta) occur, and the wall hosts nano-sized domains and dipole vortices. Adapted from [5].

process that is not observed in the bulk [5]. As a consequence, the moving walls host nano-sized domains that are polarized perpendicular to the field (shown in blue and magenta). These regions are separated by one-dimensional domain walls and polarization vortices.

Alternatively, an external field can also be used to induce dense domain walls. Figure 2 shows an example of $PbTiO_3$ in a field along [110]. Since the polarization along this direction is unfavorable, stripe domains with polarization along [100] and [010] are formed, separated by domain walls with distances of only a few unit cells [6].

Even more exciting than moving and writing domain walls uniformly in the materials, point defects allow to manipulate the wall motion on the nanoscale. Particularly, point defects in acceptor-doped materials, as shown in Figure 3 (a), can act as local pinning centers. If the defects are homogenously distributed in the material, they systematically reduced the domain wall velocity for a given field strength. Interestingly, the underlying interaction between the walls and the defect is short-ranged, and the primary factor limiting the motion is the defect-free area ahead of the wall [7].

For example, Figure 3 (b)—(c) show the motion of a tetragonal domain wall in $BaTiO_3$. Initially, the wall moves freely through the system (blue to purple lines). In the plane marked by an orange line, defect dipoles corresponding to 3.5 % Cu doping are introduced. At this defect-rich plane, most wall segments are pinned by the defect configuration. However, already a defect-free area of about 4 times 40 unit cells perpendicular or along the polarization direction, respectively, can be crossed locally. Once a wall segment has passed the defect-rich plane, there is no long-range interaction and this segment continues to move freely (red to green). The engineering of the defect distribution can thus control the wall motion on the nano-scale.

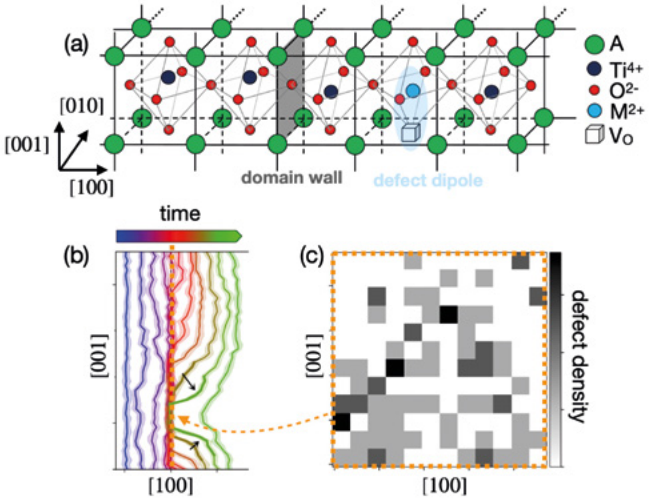

Figure 3: Domain wall pinning and depinning at point defects: (a) Atomistic picture of the tetragonal phase of $ATiO_3$ (Pb or Ba) with a domain wall (gray plane) and a defect dipole (pair of acceptor dopant M^{2+} replacing Ti^{4+} and an oxygen vacancy). (b) Time evolution of the mean wall position during field-induced motion (colors). At the orange plane with defect distribution shown in (c), wall segments are pinned, while other segments can penetrate defect-free areas. Adapted from [7].

REFERENCES:

1 Whatmore R., et al., APL Materials (2021), 9, 070401.
2 Acosta A., et al., Applied Physics Reviews (2017), 4, 041305.
3 Catalan G., et al., Reviews of Modern Physics (2019), 84, 119.
4 Grünebohm A., et al., Journal of Physics: Condensed Matter (2021), 34, 073002.
5 Khachaturyan R., et al., Physical Review Materials (2024), 8, 024403.
6 Hsu L.-T., et al., Physical Review Materials (2024), 8, 094408.
7 Teng S. H., et al., Journal of Applied Physics (2025), 137, 000000.

Materials
Research
Department

CONTACT

Materials Research Department
Universitätsstr. 150
D-44801 Bochum

@ mrd@rub.de
↗ www.mrd.rub.de